Geology

Lithospheric convective instability could induce creep along part of the San Andreas fault

Laetitia Le Pourhiet and Jason Saleeby

Geology published online 11 July 2013;
doi: 10.1130/G34244.1

Email alerting services click www.gsapubs.org/cgi/alerts to receive free e-mail alerts when new articles cite this article

Subscribe click www.gsapubs.org/subscriptions/ to subscribe to Geology

Permission request click http://www.geosociety.org/pubs/copyrt.htm#gsa to contact GSA

Copyright not claimed on content prepared wholly by U.S. government employees within scope of their employment. Individual scientists are hereby granted permission, without fees or further requests to GSA, to use a single figure, a single table, and/or a brief paragraph of text in subsequent works and to make unlimited copies of items in GSA's journals for noncommercial use in classrooms to further education and science. This file may not be posted to any Web site, but authors may post the abstracts only of their articles on their own or their organization's Web site providing the posting includes a reference to the article's full citation. GSA provides this and other forums for the presentation of diverse opinions and positions by scientists worldwide, regardless of their race, citizenship, gender, religion, or political viewpoint. Opinions presented in this publication do not reflect official positions of the Society.

Notes

Advance online articles have been peer reviewed and accepted for publication but have not yet appeared in the paper journal (edited, typeset versions may be posted when available prior to final publication). Advance online articles are citable and establish publication priority; they are indexed by GeoRef from initial publication. Citations to Advance online articles must include the digital object identifier (DOIs) and date of initial publication.

© Geological Society of America

THE GEOLOGICAL SOCIETY OF AMERICA

Geology, published online on 11 July 2013 as doi:10.1130/G34244.1

Lithospheric convective instability could induce creep along part of the San Andreas fault

Laetitia Le Pourhiet[1,2] and Jason Saleeby[3]

[1]Université Pierre-et-Marie-Curie-Paris 06, Institut des Sciences de la Terre, Paris F-75005, France

[2]CNRS, Unité Mixte de Recherche 7193, Paris F-75005, France

[3]Division of Earth and Planetary Sciences, California Institute of Technology, Pasadena, California 91125, USA

ABSTRACT

Along the western border of the Sierra Nevada microplate, the San Andreas fault (California, United States) is comprised of three segments. Two (north and south segments) are locked and support large earthquakes (e.g., the M 7.7 1906 San Francisco and the M 7.8 1857 Fort Tejon earthquakes), while the central segment, from Parkfield to San Juan Bautista, is creeping. Based on mechanical models, we show that the late Pliocene–Quaternary convective removal (delamination) of the southern Sierra Nevada mantle lithosphere and associated uplift of the Sierra Nevada Mountains causes the Great Valley upper crust to deform by flexure and buckling. Additional three-dimensional flexural models imply that the local flexural bulge overlaps with the creeping segment of the fault system, while geological observations indicate that the local weakening of the San Andreas fault started at the same time that the Sierra Nevada started its recent phase of uplift. We argue that bending stresses promote lithostatic pore pressure to occur in the depth range of 7–15 km, causing the effective strength of the fault to vanish, and locally favoring creep. Our results suggest for the first time that earthquake cycles along a major plate boundary may be influenced by convective instabilities in the adjacent upper mantle.

INTRODUCTION

Between 36°N and 37°N, where the Sierra Nevada mountain range (California, United States) reaches its highest elevations, Quaternary strata of the Great Valley embay the flank of the range's western foothills (Saleeby and Foster, 2004; Clark et al., 2005; section a-a′ in Fig. 1), and neither these strata nor the adjacent basement surface exhibit west tilt, as recorded elsewhere (Unruh, 1991; section b-b′ in Fig. 1). This geomorphic anomaly coincides with the surface projection of a prominent, steeply southeast-plunging, cylindrical-shaped, positive-seismic-velocity anomaly that extends to ~250 km deep in the upper mantle, named the Isabella anomaly (Fig. 1; Jones et al., 1994). For the sake of simplicity, we refer to the anomaly herein as a "drip," and its downward forces on the lithosphere as "drip pull."

The kinematics and timing of extension along the Eastern Sierra fault system, recent uplift of the Sierra Nevada, and the present-day drip can be explained by thermomechanical models of convective removal of the high-density root of the southern Sierra Nevada batholith (Le Pourhiet et al., 2006). In these models, once removed from beneath the batholith, the dense drip remains partially coupled to the Great Valley crust, and its "pull" along with the increase in gravitational potential energy created by the uplift of the Sierra Nevada causes the Great Valley upper crust to deform by flexure and crustal-scale buckling.

The integrated strength of the Great Valley crust controls the wavelength of the deflection (Le Pourhiet et al., 2006), with the principal subsidence node corresponding to Tulare Basin, and related uplift nodes occurring along the eastern Sierra Nevada and central Coast Ranges (Fig. 1). Additional thermomechanical modeling experiments and supporting observational data (Saleeby et al., 2012, 2013) show that a relatively weak Great Valley crust simultaneously produces the measured amounts of subsidence in Tulare Basin, and uplift of the adjacent Sierra Nevada (Fig. 1). Most pertinent to this study is that the orientation of stress in our most successful model (Fig. 2) indicates that only the upper 10–15 km of the crust deforms by flexure, and that a flexural bulge is located 150 km west of Tulare Basin. This flexural bulge coincides with the central Coast Ranges uplift,

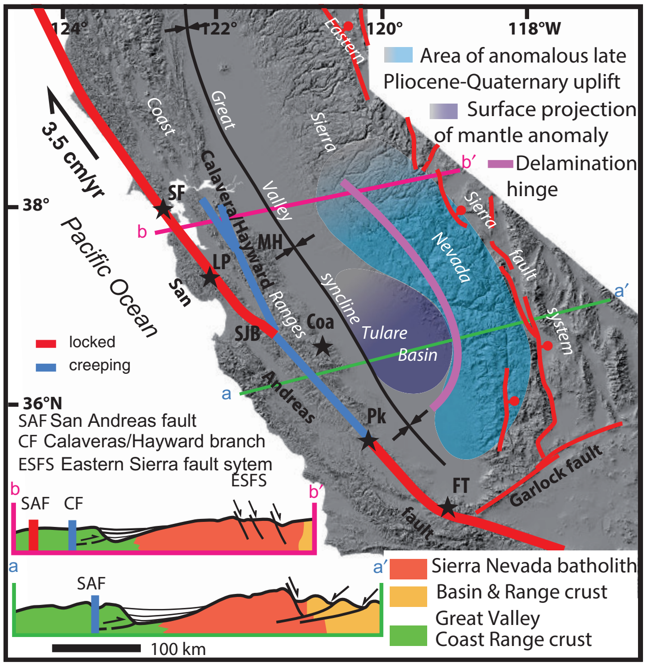

Figure 1. Digital elevation model of central California (United States) showing principal features of Sierra Nevada microplate, and principal segments of San Andreas fault system. Upper crustal structure sections a-a′ and b-b′ diagrammatically show contrasts in eastern Great Valley stratigraphic relations with the Sierran basement, topographic profiles, and Eastern Sierra fault system (ESFS) geometry. Listric normal faults of the system, rooted beneath the Sierra Nevada, are dynamically linked to the high-seismic-velocity mantle anomaly concentrated beneath Tulare Basin (Le Pourhiet et al., 2006). Profile a-a′ corresponds to the thermomechanical model trace. Black stars denote earthquake epicenters: SF—San Francisco, 1906; LP—Loma Prieta, 1989; Coa—Coalinga, 1983; FT—Fort Tejon, 1857; MH—Morgan Hill, 1984; Pk—Parkfield, 2004. SJB—San Juan Bautista. Compiled after Saleeby et al. (2012, 2013).

and overlaps with the creeping segment of the San Andreas fault. We focus on the three-dimensional (3-D) shape of this flexural bulge, and pursue its potential influence on the creeping section the San Andreas fault.

3-D Plate Deflection

A compilation of seismic imaging data for the drip reveals its 3-D geometry, and shows that asthenosphere has ascended to Moho depths beneath the adjacent Sierra Nevada where mantle lithosphere of the drip has been removed (Saleeby et al., 2012). This compilation also shows that the mobilized material has been concentrated into a drip that extends off the southern portion of the residual mantle lithosphere that remains attached to the crust. The surface projection of the drip is shown in Figure 1, along with the surface trace of the delamination hinge, which marks the surface projection of the current locus of separation between the mobilized mantle lithosphere and the crust. Noting that delamination appears to be restricted to the southern Sierra Nevada (Fig. 1) we use the distribution of the drip and the attached (remnant) mantle lithosphere west of the

© 2013 Geological Society of America. For permission to copy, contact Copyright Permissions, GSA, or editing@geosociety.org.

Geology, published online on 11 July 2013 as doi:10.1130/G34244.1

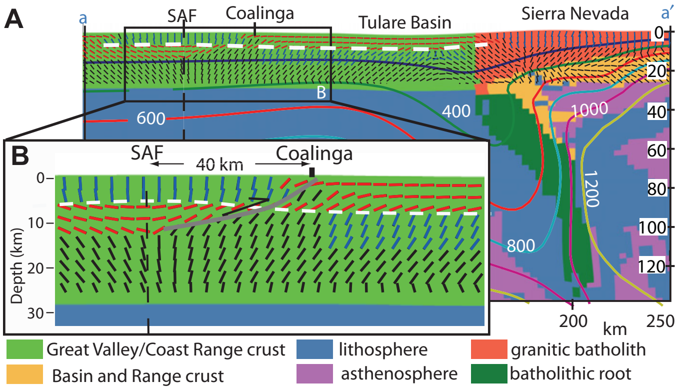

Figure 2. Results of thermomechanical modeling of southern Sierra Nevada (California) convective instability (Le Pourhiet et al., 2006; Saleeby et al., 2012). Short dashes indicate the orientation of maximum principal stress in the crust (blue is vertical, red is horizontal); white dashed line indicates effective neutral axis. A: Isotherms (in °C). B: Enlargement of stress orientation in the Great Valley. Gray line is active thrust rooting into the San Andreas fault. Colors for Great Valley and batholitic crusts are only for visualization and do not mark any mechanical contrast. Batholithic root (green) represents eclogitic residues/cumulates of the overlying batholith that have progressively delaminated from east to west over Pliocene–Quaternary time, with the locus of separation projected onto Figure 1 as the delamination hinge trace. SAF—San Andreas fault.

delamination hinge to compute anomalous buoyancy forces exerted by columns of mantle rocks (Table 1) to infer the map distribution of contemporary loads (*Pb*) acting on the crust by drip pull (Fig. 3A). Using the finite element method (Zienkievicz and Taylor, 2000) we model vertical displacement of the crust (*w*) resulting from flexure:

$$\frac{ET_e^3}{12\left(1-\nu^2\right)}\left(\frac{\partial^4 w}{\partial x^4}+2\frac{\partial w^4}{\partial x^2\,\partial y^2}+\frac{\partial^4 w}{\partial y^4}\right)+\Delta\rho g w = Pb, \qquad (1)$$

assuming an acceleration of gravity, g = 10 m/s^2 and a difference of density $\Delta\rho$ = 1500 kg/m^3 between the drip and infilling asthenosphere. E is Young modulus and T_e is effective elastic thickness. The four sides of the plate are constrained by simple support (w = 0). The model surface is 1000 × 1000 km, discretized into 10 km^2 elements, large enough that the bending moment is effectively zero on the edges (Fig. 3B).

In the thermomechanical models, the upper crust deforms by flexure down to 15 km (Fig. 2). Using the same Young modulus E = 75 GPa, but neglecting plastic yielding and viscous creep in the flexural model, we approximate the effective elastic thickness (T_e) to be <15 km in order to produce a wavelength similar to that of the thermomechanical model. With T_e = 9 km, the predictions for Quaternary uplift and subsidence for Tulare Basin and its margins satisfy depositional and exhumation data (Saleeby et al., 2013). This value is between T_e estimates reported for the Sierra Nevada (5–10 km) and for the Great Valley (10–20 km) by Lowry and Pérez-Gussinyé (2011). The model in Figure 3B produces an elliptical flexural bulge, with a long axis intersecting at a low angle to the creeping segment of the San Andreas fault, as well as the creeping Calaveras-Hayward branch of the fault system.

COULD BENDING PROMOTE CREEP?

Forces Acting on the San Andreas Fault System

The thermomechanical model implies that crustal bending accommodates the compressional stresses generated by the gravitational potential of the Sierra Nevada together with the drip pull. However, the fault is also subjected to kinematic forcing, which imposes a large component of shear, and

TABLE 1. ESTIMATION OF COLUMN LOADS, *Pb*

	a	b	c
Density anomaly (k gm^{-3})	20	40	–10
Column thickness (km)	225	75	75
Loads (MPa)	30	20	–20

Note: a, b, and c refer to the areas designated in Figure 3A.

a subsidiary component of fault normal shortening caused by the obliquity of plate motion. To simplify the analysis, we assume that buckling prevails over pure shear thickening to accommodate this shortening (McAdoo et al., 1978). This assumption is, to the first order, consistent with the mode of shortening across the Coast Ranges (Mount and Suppe, 1987; Titus et al., 2011), as it implies the formation of crustal-scale pop-up with blind thrust faults (Gerbault et al., 1999) that root into the San Andreas fault, such as those responsible for the Coalinga earthquake (Wentworth and Zoback, 1989).

Following Rice (1992), we consider the fault as a thick elastoplastic media in which discrete slip planes are embedded. The fault zone is weaker and less permeable than the adjacent nondeformed rocks due to hydration and damage zone fabric. These factors affect the intrinsic rock properties adjacent to the fault, but our analysis also reveals a critical relationship between flexural deformation and fluid pressure that must be considered as well.

Bending and Fluid Pressure

The opening of joints causes a drastic increase in permeability and thus controls the maximum sustainable fluid pressure to first order when rock permeability is very low relative to joints. Joints exist in all direction in rocks, but they are not necessarily open and filled with fluids if their normal direction diverges from the minimum principal stress. In the vicinity of the San Andreas fault, the minimum stress ($\sigma_{H_{min}}$) is horizontal and parallel to the fault (Liu et al., 1997), and thus opened joints should be vertical and normal to the fault sustaining a hydrostatic fluid pressure.

In the extrados of the flexure, bending stresses decrease the horizontal stress and the fluid pressure gradient remains hydrostatic. However,

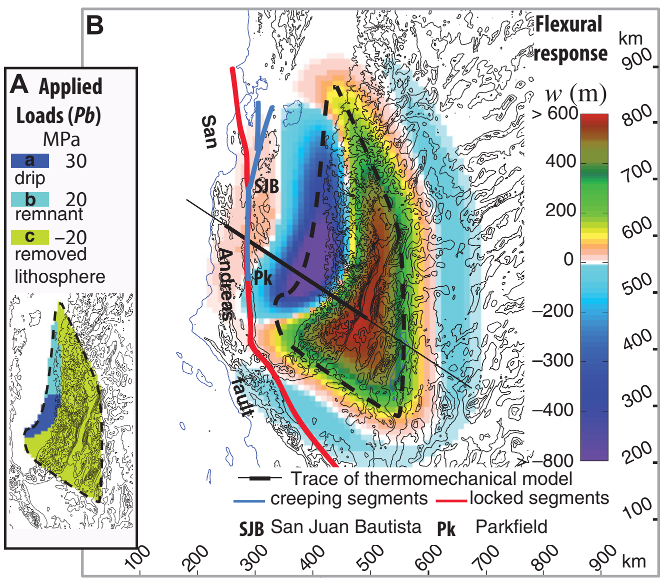

Figure 3. A: Distribution of the anomalous load related to Sierra Nevada mantle drip (a, b, and c refer to Table 1). B: Map of vertical deflection for a two-dimensional flexural model, with the model domain lying within the area of the gray box. Creeping segments (thick blue lines) are in the area of upward bending. Black dashed line outlines the area where the anomalous load is applied, as in A. Thick part of black line, representing trace of thermomechanical model, corresponds to Figure 2A cross section.

in the intrados of flexure, bending stresses increase the horizontal stress components and the vertical stress (σ_V) becomes the minimum principal stress. In these conditions, only horizontal joints may open to drain fluids, and pore fluid pressure can equate to the magnitude of vertical stress, even for drained conditions (Sibson, 2003), so that lithostatic fluid pressure may be maintained. Bending therefore provides a mechanism to maintain lithostatic fluid pressure in the flexural intrados.

Effective Elastic Strength of the Fault Zone

Following Burov and Diament (1995), yield strength envelopes determine where the fault-hosting rock column is effectively elastic when subjected to static flexural deformation at long time scales. The envelopes account for a null effective friction in domains that sustain lithostatic pressure due to the bending stresses, and a regular depth-dependent yield strength (with a static friction of 0.3–0.6) in domains of the model that can only sustain hydrostatic fluid pressure (Fig. 4).

Depending on the polarity of bending, the integrated elastic strength and the depth of the maximum elastic strength vary. For downward flexural bending, the faulted rock column possesses a larger integrated elastic strength, and its maximum elastic strength is located at the brittle-ductile transition. Oppositely, for an upward flexural bending, the integrated elastic strength is lowered and the maximum elastic strength is located close to the neutral axis.

Impact of Long-Term Strength on Discrete Slip Events

Applying a kinematic forcing to these two fault segments, we can discuss how stress can evolve with displacement during the seismic cycle. Between each slip event, the elastic core of the fault deforms elastically, storing mechanical energy that will be restored during the next slip event. The amount of elastic strain that the fault can restore as mechanical energy during slip determines the moment magnitude of the event (seismic or not).

When the elastic shear stress exceeds the static friction at the strongest point on a vertical profile (indicated by stars in Fig. 4), slip occurs on a discrete fault plane. According to rate and state formulation, slip is aseismic when effective stress is small (e.g., at high pore pressure, or close to the surface), or seismic when rock friction exhibits a velocity-strengthening behavior (Scholz, 1998). Depending on the polarity of bending, the fault can produce numerous repeated small shallow slip events (Fig. 4A) or fewer large deeper events (Fig. 4B).

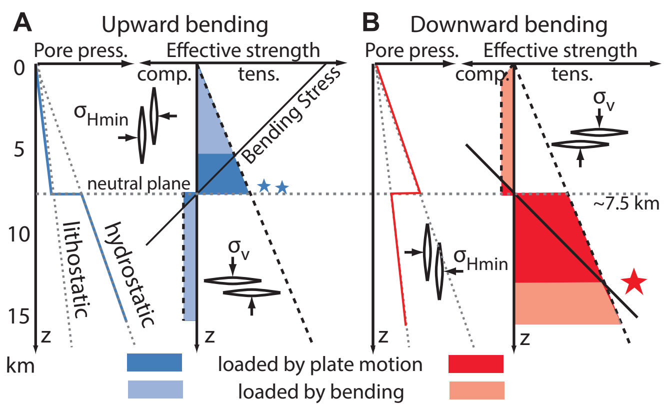

Figure 4. Diagrammatic strength profiles for segments of a fault located in contrasting areas of upward bending (A) and downward bending (B), and representation of the orientation of the resulting opened joints. Strength is constant with depth, and low in the area where elevated pore fluid pressure is promoted by horizontal jointing, and follows depth-dependent yield stress where vertical joints predominate. Brittle-ductile transition is at bottom of profiles. Stars denote depths where the largest slip events are predicted to initiate (comp.—compression; tens.—tension; σ_V—lithostatic pressure; $\sigma_{H_{min}}$—minimum horizontal stress; Pore press.—pore pressure).

The creeping segment of the San Andreas fault, and its creeping Calaveras-Hayward branch, are located where the crust buckles up in response to the drip load (Fig. 3). In these areas, the bimodal depth distribution of hypocenters (Thurber et al., 2006), the large slip patches inferred at ~7 km during the repeated ~M 6 events (Langbein et al., 2006), and the similar shallow hypocenter (8 km) for the Mw 6.2 Morgan Hills earthquake (Bakun et al., 1984) are consistent with the model predictions (Fig. 4A). The deep hypocenter (18 km) of the 1989 Loma Prieta earthquake (~M = 7.1; Dietz and Ellsworth, 1990) is consistent with the strongest part of the crust being located near the brittle-ductile transition along a locked segment of the fault (Figs. 1 and 4B).

DISCUSSION

Our model pertains to the family of faults characterized as weak faults within strong crust. Such fault behavior requires the effective friction to drop to 0.1, promoted by low rock friction and/or high fluid pressure. Reduction of rock friction down to 0.3 or 0.4 is readily achieved by integrating the effects of common clay minerals like smectite (Numelin et al., 2007), damage zone fabric (Collettini et al., 2009), or gouge compaction (Lecomte et al., 2011). The two latter mechanisms may also accommodate localized normal shortening proximal to the fault zone (1–5 km), as inferred from GPS and field data (Titus et al., 2011), and the promotion of smaller earthquakes (Lecomte et al., 2012) and creep (Sleep and Blanpied, 1992). None of these mechanisms alone can drop the friction to 0.1 unless the clay mineral is talc (Lockner et al., 2011). The talc found at the San Andreas Fault Observatory at Depth (SAFOD; Moore and Rymer, 2007) belongs to a serpentinized body, which only extends from 3 to 5 km depth (McPhee et al., 2004), and therefore it can explain surface creep but it cannot explain creep at greater depth.

Despite their inherent simplicity, the fluid overpressure models for the creeping segment (e.g., Rice, 1992) were partly rejected after a hydrostatic fluid pressure gradient was found in a SAFOD drill hole down to 3.2 km depth (Tembe et al., 2009). However, this observation does not preclude that lithostatic pore pressure exists deeper in the rock column, as our model predicts. Moreover, the local seismic anisotropy signal that supports open fluid-filled vertical joints near the surface vanishes at depths >7–8 km (Cochran et al., 2006; Liu et al., 1997), while the resistivity profile near Parkfield shows a clear polarity reversal from high resistivity (low fluid content) at depth beneath the locked segment to low resistivity (high fluid contents) at depth beneath the creeping segment (Becken et al., 2011). The lack of a mantle helium signature at the SAFOD and its occurrence in the adjacent Great Valley (Wiersberg and Erzinger, 2007) are also consistent with the presence of a horizontal fluid barrier beneath the creeping segment.

Miocene age (older than 5.6 Ma) folds along the creeping segment have axes ~30° oblique to the fault, while Pliocene–Quaternary (younger than 3.5 Ma) fold axes are nearly parallel to the fault (Mount and Suppe, 1987). This sudden change in fold orientations adjacent to the fault cannot be explained by passive rotation, but rather by a local drop of static friction along the fault at ca. 4 Ma (Mount and Suppe, 1987; Chéry et al., 2001). This change in orientation cannot be explained by a change in the intrinsic properties of the fault rocks, or by any documented change in the plate motion. The only significant geological event recognized at this time is the convective removal of the southern Sierra Nevada mantle lithosphere (Saleeby et al., 2003, 2013), which we show here results in localized flexural bulging.

CONCLUSIONS

Our self-consistent thermomechanical modeling of mantle lithosphere removal and uplift of the Sierra Nevada (Le Pourhiet et al., 2006), as well as the resulting subsidence and uplift patterns (Saleeby et al., 2013), indicate that this event induces crustal flexure and buckling rather than pure shear deformation west of the Sierra Nevada mountain range. Our flexural model of the response of the crust to the internal loads generated by the southern Sierra Nevada drip strongly suggests that the delamination of the Sierra

Nevada batholitic root since ca. 4 Ma is responsible for flexural deformation that corresponds to the geologically recent uplift and subsidence patterns of the southern Sierra–Great Valley region, and adds an uplift component in the adjacent Coast Ranges where cut by the San Andreas fault system.

We show that where the crust responds to the drip by upward bending, faults of the San Andreas system are creeping, and further provide mechanical insights on how bending stresses could be a major factor in promoting long-lived creep along the system where it is affected by the upward bending. Our model provides the first coherent large-scale geodynamic explanation for the location and length scale of the creeping segment of the San Andreas fault system, and for the timing of the initiation of fault-parallel folding along this segment of the system.

ACKNOWLEDGMENTS

This research was supported in part by a grant from the George and Betty Moore Foundation and INSU (Institut National des Sciences de l'Univers). This is contribution 104 of the California Institute of Technology (CalTech) Tectonics Observatory, and contribution 10016 of the Division of Geological and Planetary Science, CalTech. We thank three anonymous reviewers for the in-depth reviews that greatly improved the clarity of this manuscript.

REFERENCES CITED

Bakun, W.H., Clark, M.M., Cockerham, R.S., Ellsworth, W.L., Lindh, A.G., Prescott, W.H., Shakal, A.F., and Spudich, P., 1984, The 1984 Morgan Hill, California, earthquake: Science, v. 225, p. 288–291, doi:10.1126/science.225.4659.288.

Becken, M., Ritter, O., Bedrosian, P.A., and Weckmann, U., 2011, Correlation between deep fluids, tremor and creep along the central San Andreas fault: Nature, v. 480, p. 87–90, doi:10.1038/nature10609.

Burov, E.B., and Diament, M., 1995, The effective elastic thickness (T_e) of continental lithosphere: What does it really mean?: Journal of Geophysical Research, v. 100, p. 3905–3927, doi:10.1029/94JB02770.

Chéry, J., Zoback, M.D., and Hassani, R., 2001, An integrated mechanical model of the San Andreas fault in central and northern California: Journal of Geophysical Research, v. 106, 22051, doi:10.1029/2001JB000382.

Clark, M.K., Maheo, G., Saleeby, J., and Farley, K.A., 2005, The non-equilibrium landscape of the southern Sierra Nevada, California: GSA Today, v. 15, no. 9, p. 4–10, doi:10.1130/1052-5173(2005)015[4:TNLOTS]2.0.CO;2.

Cochran, E.S., Li, Y.G., and Vidale, J.E., 2006, Anisotropy in the shallow crust observed around the San Andreas fault before and after the 2004 M 6.0 Parkfield earthquake: Seismological Society of America Bulletin, v. 96, p. S364–S375, doi:10.1785/0120050804.

Collettini, C., Niemeijer, A., Viti, C., and Marone, C., 2009, Fault zone fabric and fault weakness: Nature, v. 462, p. 907–910, doi:10.1038/nature08585.

Dietz, L.D., and Ellsworth, W.L., 1990, The October 17, 1989, Loma Prieta, California, earthquake and its aftershocks: Geometry of the sequence from high-resolution locations: Geophysical Research Letters, v. 17, p. 1417–1420, doi:10.1029/GL017i009p01417.

Gerbault, M., Burov, E.B., Poliakov, A., and Daignières, M., 1999, Do faults trigger folding in the lithosphere?: Geophysical Research Letters, v. 26, p. 271–274, doi:10.1029/1998GL900293.

Jones, C.H., Kanamori, H., and Roecker, S.W., 1994, Missing roots and mantle "drips": Regional P_n and teleseismic arrival times in the southern Sierra Nevada and vicinity, California: Journal of Geophysical Research, v. 99, p. 4567–4601, doi:10.1029/93JB01232.

Langbein, J., Murray, J.R., and Snyder, H.A., 2006, Coseismic and initial postseismic deformation from the 2004 Parkfield, California, earthquake, observed by Global Positioning System, electronic distance meter, creepmeters, and borehole strainmeters: Seismological Society of America Bulletin, v. 96, p. S304–S320, doi:10.1785/0120050823.

Lecomte, E., Le Pourhiet, L., Lacombe, O., and Jolivet, L., 2011, A continuum mechanics approach to quantify brittle strain on weak faults: Application to the extensional reactivation of shallow dipping discontinuities: Geophysical Journal International, v. 184, p. 1–11, doi:10.1111/j.1365-246X.2010.04821.x.

Lecomte, E., Le Pourhiet, L., and Lacombe, O., 2012, Mechanical basis for slip along low-angle normal faults: Geophysical Research Letters, v. 39, L03307, doi:10.1029/2011GL050756.

Le Pourhiet, L., Gurnis, M., and Saleeby, J., 2006, Mantle instability beneath the Sierra Nevada mountains in California and Death Valley extension: Earth and Planetary Science Letters, v. 251, p. 104–119, doi:10.1016/j.epsl.2006.08.028.

Liu, Y., Crampin, S., and Main, I., 1997, Shear-wave anisotropy: Spatial and temporal variations in time delays at Parkfield, central California: Geophysical Journal International, v. 130, p. 771–785, doi:10.1111/j.1365-246X.1997.tb01872.x.

Lockner, D.A., Morrow, C., Moore, D., and Hickman, S., 2011, Low strength of deep San Andreas fault gouge from SAFOD core: Nature, v. 472, p. 82–85, doi:10.1038/nature09927.

Lowry, A.R., and Pérez-Gussinyé, M., 2011, The role of crustal quartz in controlling Cordilleran deformation: Nature, v. 471, p. 353–357, doi:10.1038/nature09912.

McAdoo, D.C., Caldwell, J.G., and Turcotte, D.L., 1978, On the elastic-perfectly plastic bending of the lithosphere under generalized loading with application to the Kuril Trench: Royal Astronomical Society Geophysical Journal, v. 54, p. 11–26, doi:10.1111/j.1365-246X.1978.tb06753.x.

McPhee, D.K., Jachens, R.C., and Wentworth, C.M., 2004, Crustal structure across the San Andreas fault at the SAFOD site from potential field and geologic studies: Geophysical Research Letters, v. 31, L12S03, doi:10.1029/2003GL019363.

Moore, D.E., and Rymer, M.J., 2007, Talc-bearing serpentinite and the creeping section of the San Andreas fault: Nature, v. 448, p. 795–797, doi:10.1038/nature06064.

Mount, V.S., and Suppe, J., 1987, State of stress near the San Andreas fault: Implications for wrench tectonics: Geology, v. 15, p. 1143–1146, doi:10.1130/0091-7613(1987)15<1143:SOSNTS>2.0.CO;2.

Numelin, T., Marone, C., and Kirby, E., 2007, Frictional properties of natural fault gouge from a low-angle normal fault, Panamint Valley, California: Tectonics, v. 26, TC2004, doi:10.1029/2005TC001916.

Rice, J.R., 1992, Fault stress states, pore pressure distributions, and the weakness of the San Andreas fault: International Geophysics, v. 51, p. 475–503, doi:10.1016/S0074-6142(08)62835-1.

Saleeby, J., and Foster, Z., 2004, Topographic response to mantle lithosphere removal in the southern Sierra Nevada region, California: Geology, v. 32, p. 245–248, doi:10.1130/G19958.1.

Saleeby, J., Ducea, M., and Clemens-Knott, D., 2003, Production and loss of high-density batholithic root, southern Sierra Nevada, California: Tectonics, v. 22, 1064, doi:10.1029/2002TC001374.

Saleeby, J., Le Pourhiet, L., Saleeby, Z., and Gurnis, M., 2012, Epeirogenic transients related to mantle lithosphere removal in the southern Sierra Nevada region, California, Part I: Implications of thermo-mechanical modeling: Geosphere, v. 8, p. 1286–1309, doi:10.1130/GES00746.1.

Saleeby, J., Saleeby, Z., and Le Pourhiet, L., 2013, Epeirogenic transients related to mantle lithosphere removal in the southern Sierra Nevada region, Part II: Implications of rock uplift and basin subsidence relations: Geosphere, v. 9, p. 1–32, doi:10.1130/GES00816.1.

Scholz, C., 1998, Earthquakes and friction laws: Nature, v. 391, p. 37–42, doi:10.1038/34097.

Sibson, R.H., 2003, Brittle-failure controls on maximum sustainable overpressure in different tectonic regimes: American Association of Petroleum Geologists Bulletin, v. 87, p. 901–908, doi:10.1306/01290300181.

Sleep, N.H., and Blanpied, M.L., 1992, Creep, compaction and the weak rehology of major faults: Nature, v. 359, p. 687–692, doi:10.1038/359687a0.

Tembe, S., Lockner, D., and Wong, T., 2009, Constraints on the stress state of the San Andreas fault with analysis based on core and cuttings from San Andreas Fault Observatory at Depth (SAFOD) drilling phases 1 and 2: Journal of Geophysical Research, v. 114, B11401, doi:10.1029/2008JB005883.

Thurber, C., Zhang, H., Waldhauser, F., Hardebeck, J., Michael, A., and Eberhart-Phillips, D., 2006, Three-dimensional compressional wavespeed model, earthquake relocations, and focal mechanisms for the Parkfield, California, region: Seismological Society of America Bulletin, v. 96, p. S38–S49, doi:10.1785/0120050825.

Titus, S.J., Dyson, M., DeMets, C., Tikoff, B., Rolandone, F., and Bürgmann, R., 2011, Geologic versus geodetic deformation adjacent to the San Andreas fault, central California: Geological Society of America Bulletin, v. 123, p. 794–820, doi:10.1130/B30150.1.

Unruh, J.R., 1991, The uplift of the Sierra Nevada and implications for late Cenozoic epeirogeny in the western Cordillera: Geological Society of America Bulletin, v. 103, p. 1395–1404, doi:10.1130/0016-7606(1991)103<1395:TUOTSN>2.3.CO;2.

Wentworth, C.M., and Zoback, M.D., 1989, The style of late Cenozoic deformation at the eastern front of the California Coast Ranges: Tectonics, v. 8, p. 237–246, doi:10.1029/TC008i002p00237.

Wiersberg, T., and Erzinger, J., 2007, A helium isotope cross-section study through the San Andreas fault at seismogenic depths: Geochemistry Geophysics Geosystems, v. 8, Q01002, doi:10.1029/2006GC001388.

Zienkievicz, O.C., and Taylor, R.L., 2000, The finite element method: Volume 2, Solid mechanics (fifth edition): Oxford, UK, Butterworth-Heinemann, 459 p.

Manuscript received 18 November 2012
Revised manuscript received 16 April 2013
Manuscript accepted 5 May 2013

Printed in USA